Nanostructured Electrodes

DOI: 10.1002/anie.200704287

Superior Storage Performance of a Si@SiO_x/C Nanocomposite as Anode Material for Lithium-Ion Batteries**

Yong-Sheng Hu, Rezan Demir-Cakan, Maria-Magdalena Titirici,* Jens-Oliver Müller, Robert Schlögl, Markus Antonietti, and Joachim Maier**

Rechargeable lithium-ion batteries are essential to portable electronic devices. Owing to the rapid development of such equipment there is an increasing demand for lithium-ion batteries with high energy density and long cycle life. For high energy density, the electrode materials in the lithium-ion batteries must possess high specific storage capacity and coulombic efficiency. Graphite and $LiCoO_2$ are normally used and have high coulombic efficiencies (typically $>90\,\%$) but rather low capacities (372 and 145 $mA\,h\,g^{-1}$, respectively).[1–5] Various anode materials with improved storage capacity and thermal stability have been proposed for lithium-ion batteries in the last decade. Among these, silicon has attracted great interest as a candidate to replace commercial graphite materials owing to its numerous appealing features: it has the highest theoretical capacity ($Li_{4.4}Si \approx 4200\ mA\,h\,g^{-1}$) of all known materials, and is abundant, inexpensive, and safer than graphite (it shows a slightly higher voltage plateau than that of graphite as shown in Figure S1, and lithiated silicon is more stable in typical electrolytes than lithiated graphite[6]).

The practical use of Si powders as a negative electrode in lithium-ion batteries is, however, still hindered by two major problems: the low intrinsic electric conductivity and severe volume changes during Li insertion/extraction processes, leading to poor cycling performance.[7–20] Tremendous efforts have been made to overcome these problems by decreasing the particle size,[7,8a,b] using silicon-based thin films and silicon–metal alloys,[9,10,20] dispersing silicon into an inactive/active matrix,[11–19] and coating with carbon as well as using different electrolyte systems.[15,20] In these approaches a variety of composites of active and inactive materials have been widely exploited in which the inactive component plays a structural buffering role to minimize the mechanical stress induced by huge volume change of active silicon, thus preventing the deterioration of the electrode integrity.[11–19] Recent work has demonstrated that anodes made of silicon/carbon composites can combine the advantageous properties of carbon (long cycle life) and silicon (high lithium-storage capacity) to improve the overall electrochemical performance of the anode for lithium-ion batteries.[8c,9b,11–13,15–17] For example, Wilson et al. synthesized nanodispersed silicon in carbon using chemical vapor deposition (CVD) and received a reversible capacity of roughly 500 $mA\,h\,g^{-1}$.[11] Yoshio and co-workers reported that carbon-coated silicon synthesized by the thermal vapor deposition (TVD) method shows better cycling characteristics than conventional silicon anodes.[12] Guo et al. reported the production of a nanocomposite of silicon and disordered carbon using a pyrolitic process and polyvinylalcohol (PVA) as a carbon source.[13b] Carbon-coated Si nanocomposites with high capacities and high coulombic efficiencies were also prepared by Liu et al. by a spray-pyrolysis technique.[13c]

In contrast to these rather complicated high-temperature processes we report here a new, simple, and green methodology for the simultaneous coating of preformed silicon nanoparticles in a one-step procedure with a thin layer of SiO_x and carbon by the hydrothermal carbonization of glucose. This Si@SiO_x/C nanocomposite with a typical core/shell structure, which was further modified by electrochemical in situ generation of a passivated layer, shows remarkably improved lithium-storage performance in terms of high reversible lithium-storage capacity ($\approx 1100\ mA\,h\,g^{-1}$), excellent cycling performance, and high rate capability.

Carbonaceous materials can be produced using hydrothermal carbonization (HTC), which is a well-established method to create hydrophilic carbon materials starting from a water-soluble carbohydrate heated at mild temperatures (180–200 °C) in an autoclave.[21] A simplified reaction mechanism for the formation of the carbon spheres involves the dehydration of the carbohydrate in the first step and subsequent polymerization and carbonization of the thus-generated organic compounds in the second step. The resulting droplets form either the final spherical carbon particles or they can be used for nanocoating other structures.[22] Glucose, obtained from biomass, was selected as the carbon source and a silicon nanoparticle powder (20–50 nm, see Figure S2 in the Supporting Information) was used as the silicon source. This process is schematically illustrated in Figure S3 in the Supporting Information. Owing to the hydrothermal conditions, besides the carbon coating, a layer of silicon oxide (SiO_x) several nanometers thick is formed on

[*] Dr. Y.-S. Hu, Prof. Dr. J. Maier
Max-Planck-Institut für Festkörperforschung
Heisenbergstrasse 1, 70569 Stuttgart (Germany)
E-mail: yshu@engineering.ucsb.edu
s.weiglein@fkf.mpg.de

R. Demir-Cakan, Dr. M.-M. Titirici, Prof. Dr. M. Antonietti
Max-Planck-Institut für Kolloid- und Grenzflächenforschung
Wissenschaftspark Golm, 14424 Potsdam (Germany)
E-mail: Magdalena.Titirici@mpikg.mpg.de

Dr. J.-O. Müller, Prof. Dr. R. Schlögl
Fritz-Haber-Institut der Max-Planck-Gesellschaft
Faradayweg 4–6, 14195 Berlin (Germany)

[**] We thank G. Götz, M. Konuma, and A. Schulz for their technical support. We are indebted to the Max Planck Society and acknowledge support in the framework of the ENERCHEM project. We also acknowledge valuable comments from the reviewers.

Supporting information for this article is available on the WWW under http://www.angewandte.org or from the author.

the surface of silicon nanoparticles. Thermogravimetrical analysis (TGA, see Figure S4 in the Supporting Information) of the resulting sample is in good agreement with elemental microanalysis showing a carbon content of ca. 25 wt%. The X-ray diffraction (XRD) pattern of the Si@SiO_x/C nanocomposite (Figure 1a) is identical with that of the pure Si

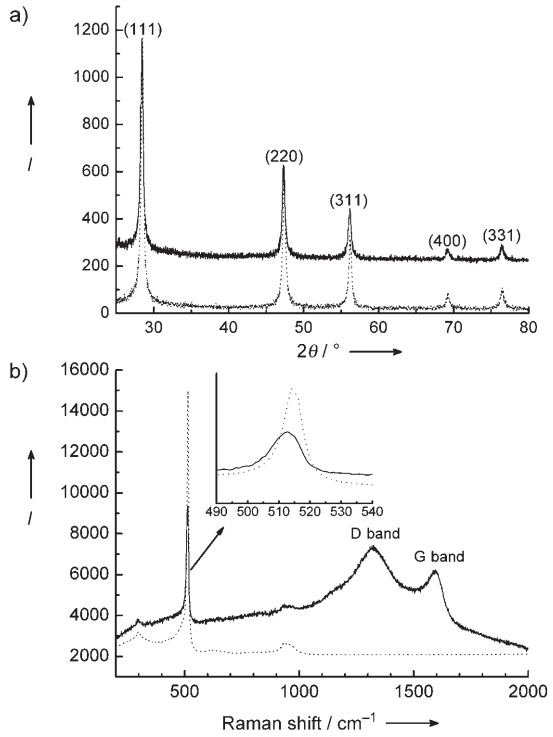

Figure 1. a) XRD patterns and b) Raman spectra of the silicon nanoparticles before and after carbon coating (solid line: Si@SiO_x/C, dotted line: Si).

nanoparticles, indicating that no SiO_x crystalline phase was formed during the hydrothermal carbonization, although as mentioned before a very thin layer of amorphous SiO_x (3–5 nm) can be detected by HRTEM and FTIR (see Figure S5 in the Supporting Information). Following the LeBail method, we deduced crystallite dimensions of about 23 nm and 24 nm for the Si nanoparticles before and after carbon coating, suggesting that the hydrothermal carbonization and high-temperature treatment do not change the crystallite size of the sample. No diffraction peaks corresponding to graphitic carbon were observed in the XRD pattern, meaning that the carbon coating is amorphous. Figure 1b shows the Raman spectra of the pure silicon nanoparticles and the Si@SiO_x/C nanocomposite; a clear difference can be observed between the two samples. In the case of the Si@SiO_x/C nanocomposite, the relative low intensity and blue shift of the band at ca. 515 cm^{-1}, which originates from the transverse optical mode, could probably be due to a phonon confinement effect[23] and/or a masking effect; this implies that the silicon nanoparticles are covered with amorphous SiO_x and a carbon layer. The Raman spectrum of the Si@SiO_x/C nanocomposite contains the characteristic wide D and G bands around 1360 and 1590 cm^{-1}, respectively, typical for amorphous carbon or disordered graphite. The large I_D/I_G ratio indicates the low graphitic degree in the hydrothermal carbon material.

Figure 2 (and Figure S6 in the Supporting Information) shows TEM micrographs of uniform spherelike particles of the Si@SiO_x/C nanocomposite with an average diameter of ca. 40 nm. Figure 2b and the inset in Figure 2a show that

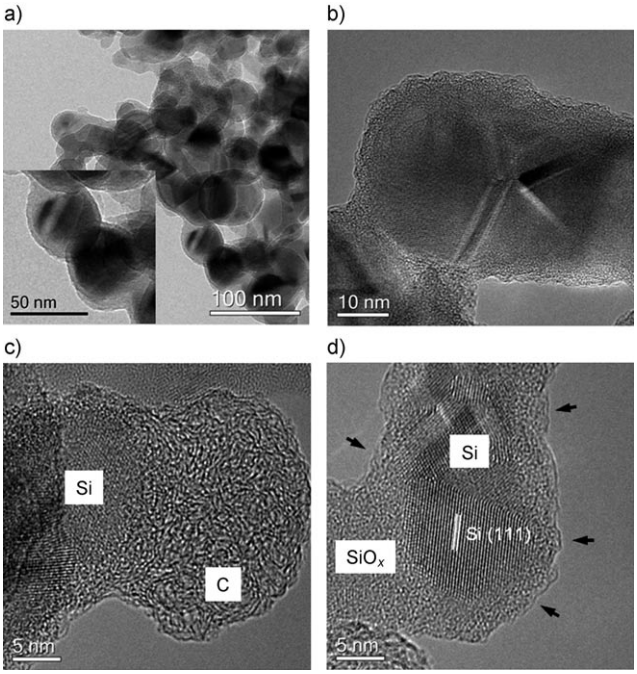

Figure 2. TEM images of the Si@SiO_x/C nanocomposite produced by hydrothermal carbonization and further carbonization at 750 °C under N_2. a) Overview of the Si@SiO_x/C nanocomposites and a TEM image at higher magnification (in the inset) showing uniform spherelike particles; b) HRTEM image clearly showing the core/shell structure; c), d) HRTEM image displaying details of the silicon nanoparticles coated with SiO_x and carbon.

these particles have a core/shell structure. The thickness of this layer forming a complete shell is around 10 nm (SiO_x and C), whereas the diameter of core is around 30–40 nm, which is very similar to the size of pure Si nanoparticles. In HRTEM images (Figure 2b–d) it is evident that the Si nanoparticles are coated with a layer of silicon oxide and a layer of carbon with varying thickness. Short, strongly bent graphene layers were observed on the surface of all of the particles (indicated by small arrows in Figure 2d). The Si powder consists of agglomerates of nanoparticles. Coating these particles may lead to a heterogeneous coverage with SiO_x and carbon, as the particles may not be perfectly dispersed during the HTC process. In these agglomerates the particles are entangled, therefore it can be observed that some silicon nanoparticles have thicker carbon coatings (Figure 2b,c) than others (Figure 2d). In Figure 2d it is apparent that the carbon coating is thin and consists of one to three grapheme layers. In summary, the HRTEM, Raman, and FTIR investigations indicate that the nanocomposite consists of a silicon core, a shell of thin amorphous SiO_x, and a carbon layer. Such a structure should be very interesting for lithium storage as it

can combine sufficient conductivity with polymerlike elasticity to withstand the deformation stresses.

The lithium-storage properties of pure Si nanoparticles and Si@SiO_x/C nanocomposite electrodes were investigated in different electrolyte systems. Figure 3a shows galvanostatic discharge/charge curves (for Li insertion/Li extraction) of pure Si nanoparticle and Si@SiO_x/C nanocomposite electrodes cycled at a current density of 150 mA g^{-1} between the voltage limits of 0.05–1 V in vinylene carbonate (VC)-free and VC-containing 1 M $LiPF_6$ in ethylene carbonate/dimethyl carbonate (EC/DMC) solution. It can be observed that pure Si nanoparticles delivery very high discharge and charge capacities of around 3200 and 1800 mA h g^{-1}, respectively, in the first cycle. However, after several cycles, the capacity rapidly decays to 20 mA h g^{-1}. When vinylene carbonate (VC) is added to the electrolyte (note that VC is widely regarded as the best agent for the formation of passivating films on the surface of electrode materials, especially for carbon materials.[15,20]), the Si nanoparticles show a slightly better cycling performance. The pure, nonpassivated Si@SiO_x/C nanocomposite also shows better cycling performance than the pure Si nanoparticles, but it still exhibits rapid capacity decay in the VC-free electrolyte (Figure 3a,b), suggesting that the SiO_x/C coating on Si nanoparticles is still not sufficient for achieving good cycling performance. Finally, when the Si@SiO_x/C nanocomposite electrode was cycled in the VC-containing electrolyte, an excellent cycling performance was achieved. The reversible capacity is as high as 1100 mA h g^{-1} at a current density of 150 mA g^{-1}, with no further decay of capacity even after 60 cycles. A large irreversible capacity was observed in the first discharge and charge process; however, after the initial cycles, the coulombic efficiency is above 99%. The irreversible capacity in the first initial cycles is an expected phenomenon in the Si-based electrodes in lithium batteries.[7–10,13–16] The initial irreversible capacity loss could mainly originate from the reduction of the electrolyte, resulting in the formation of a solid electrolyte interphase (SEI) on the surface of the active particles and/or from irreversible lithium insertion into nanocomposites. This might be overcome by preforming an artificial SEI layer (through chemical modification) on the active particles and/or prelithiating the active particles.[24]

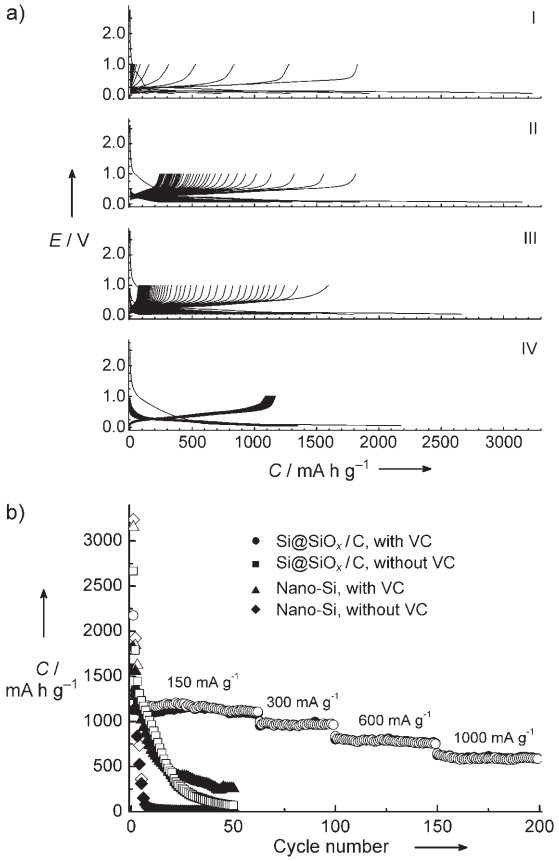

Figure 3. a) Galvanostatic discharge/charge curves (Li insertion, voltage decreases; Li extraction, voltage increases, respectively) of pure Si nanoparticles (I, II) and Si@SiO_x/C nanocomposite (III, IV) electrodes cycled at a current density of 150 mA g^{-1} between voltage limits of 0.05–1 V in VC-free (I, III) and VC-containing (II, IV) 1 M $LiPF_6$ in EC/DMC solutions. b) Cycling and rate performance of pure Si nanoparticles and Si@SiO_x/C nanocomposite electrodes cycled in VC-free and VC-containing 1 M $LiPF_6$ in EC/DMC solutions (solid symbols: charge; empty symbols: discharge.).

The Si@SiO_x/C nanocomposite electrode was also allowed to discharge/charge at higher current densities. As shown in Figure 3b and Figure S7, after the cell was cycled at a rate of 150 mA g^{-1} for 60 cycles, the current density was increased in stages to 1000 mA g^{-1}; highly stable reversible capacities around 960, 760, and 600 mA h g^{-1} were obtained at current densities of 300, 600, and 1000 mA g^{-1}, respectively. In addition, a flat voltage plateau in the discharge/charge curves was also observed even at a high current density of 1000 mA g^{-1} (see Figure S7 in the Supporting Information). These results clearly show that coating with SiO_x/C and VC plays an important role in improving the electrochemical performance of silicon electrode.

The significant improvement of the lithium-storage properties of Si@SiO_x/C nanocomposite electrode cycled in the VC-containing electrolyte is mainly related to the formation of a SEI on the surface of active particles. Careful inspection of the first discharge curves for all the samples (see Figure S8a,b in the Supporting Information) reveals significant differences among them. (The differential capacity curves for all the discharge curves are presented in Figure S8c in the Supporting Information.) In the case of pure Si nanoparticles, an irreversible reduction peak can be observed at 0.66 V in the VC-free electrolyte. This corresponds to the reductive decomposition of the EC/DMC electrolyte on the surface of Si. However, two reduction peaks at 0.98 and 0.63 V were observed in the VC-containing electrolyte. They are ascribed to the reductive decomposition of the VC and EC/DMC electrolyte, respectively. In the case of Si@SiO_x/C nanocomposite, the EC/DMC electrolyte without VC starts to decompose at 0.83 V to form a SEI on the surface of carbon instead of on Si. The VC-containing electrolyte starts to decompose at 1.2 V, which is in good agreement with previous reports.[1,15] An additional peak near 0.3 V was also observed for both samples, which is assigned to Li reacting with SiO_x to form lithium silicate.[19] These results demonstrate that both

the active coating materials and the composition of the electrolytes have a strong effect on the formation of an effective SEI structure.

To further understand the reason for the improved cyclability of the Si@SiO_x/C nanocomposite electrode in VC-containing electrolyte, electrochemcial impedance spectroscopy (EIS) measurements were performed after the first cycle. The Nyquist plots of the Si@SiO_x/C nanocomposite electrode cycled in VC-free and VC-containing electrolytes are presented in Figure 4. Both Nyquist plots consist of one

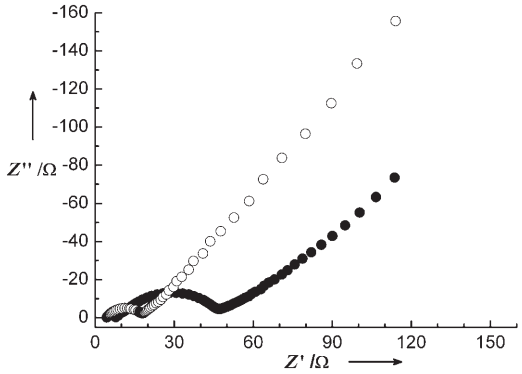

Figure 4. Nyquist plots of a Si@SiO_x/C nanocomposite electrode cycled in VC-free (empty circles) and VC-containing (solid circles) electrolytes.

depressed semicircle at high frequencies (HF) and a straight line at low frequencies. As the resistances of electrode and electrolyte are negligible, the HF semicircle should relate to properties of the SEI layer.[20] Figure 4 shows that the diameter of the HF semicircle of the Si@SiO_x/C nanocomposite electrode in VC-containing electrolyte is much larger than that in the VC-free electrolyte. This indicates that the higher resistance of the SEI layer is related to a thicker and/or denser layer structure formed in the VC-containing electrolyte. This higher resistance of the SEI layer was also reflected in the flat voltage plateau region (Li insertion into the Si) of the first discharge curve (see Figure S9 in the Supporting Information . The voltage plateau for both electrodes cycled in the VC-containing electrolyte is about 50 mV lower than when those electrodes are cycled in the VC-free electrolyte. (Note that the first discharge capacity is also lower in the same tested voltage window.) This implies a higher resistance for Li insertion into the Si and could only originate from the higher resistance of the encapsulating layer formed in the VC-containing electrolyte.

Ex situ XPS results (see Figure S10 in the Supporting Information) show that the Si 2p signal of the Si@SiO_x/C sample cycled in the VC-containing electrolyte is much weaker than that of the sample cycled in the VC-free electrolyte. However, after Ar^+ sputtering for 5 min, which is sufficient to remove the surface carbon species, both samples show a similar Si 2p signal, which indirectly confirms that the thicker and/or more dense SEI layer formed in the presence of VC. It has been reported by Aurbach and coworkers that the main compositions of SEI on the graphite electrode resulting from VC-based electrolyte are poly(alkyl lithium carbonate) species.[25] Such surface films containing polymerlike species are expected to be more cohesive and flexible, and thus provide better passivation than surface films comprising only Li salts. In the case of the Si@SiO_x/C nanocomposites, similar film formation might be expected since the surface of all of the active particles is covered by a thin layer of carbon.

From the above analyses, we can conclude that only the combination of a SiO_x-binding layer on the Si nanoparticles which adheres to an elastic, ca. 10–20-nm thick hydrothermal carbon shell, electrochemically sealed in situ in the first cycle by reaction with vinylene carbonate, can ensure a sufficiently mechanically and electrochemically stable SEI layer. This can then resist the harsh deformation processes that occur when the Si nanoparticles are loaded with Li. In this way, the structural stability of the electrode and good electronic and ionic conduction pathways are maintained, which apparently results in excellent cycling performance. The lower first discharge capacity for the Si@SiO_x/C sample cycled in the same tested voltage window in the VC-containing electrolyte (as shown in Figure S9b in the Supporting Information), which is a consequence of high polarization, is probably also responsible for the excellent cycling performance. It has been reported that capacity-limiting is one way for achieving good cycling performance of silicon electrodes.[15,26]

In summary, we have described a facile and straightforward synthesis of Si@SiO_x/C nanocomposites in water by the hydrothermal carbonization of glucose in the presence of Si nanoparticles. The resulting material shows a significantly improved lithium-storage performance in terms of highly reversible lithium-storage capacity, excellent cycling performance, and high rate capability. Although further studies are required to understand and overcome the irreversible capacity in the initial cycles, Si@SiO_x/C nanocomposites can be considered promising candidates as anode materials in lithium-ion batteries.

Experimental Section

Preparation of the Si@SiO_x/C nanocomposite: Silicon nanoparticles (1 g, 20–50 nm; Nanostructured and Amorphous Materials Inc.) were dispersed in 10 mL of water inside a Teflon inlet of a stainless-steel autoclave by sonication. After glucose (0.5 g) had been added to the dispersion, and the mixture was treated hydrothermally heated at 200 °C for 12 h. The resulting material was isolated by centrifugation and further carbonized under N_2 flow at 750 °C for 4 h in order to improve the structural order of the carbon coating.

Structural and electrochemical characterization: TEM images were recorded using an Omega 912 transmission electron microscope (Carl Zeiss, Oberkochen, Germany). A Philips TEM/STEM CM 200 FEG transmission electron microscope equipped with a field emission gun was used to study the morphology and microstructure of the Si/SiO_x/C nanocomposites. The acceleration voltage was set to 200 kV. Electronic structure measurements were performed using EELS. Spectra were recorded with the Gatan imaging filter tridiem with an energy resolution of 1 eV measured at the full width at half maximum (FWHM) of the zero loss. EFTEM maps were acquired using the same instrument. The particle size and morphology was visualised using a "Gemini" scanning electronic microscope. XRD patterns were recorded on a Philips machine using $Cu_{K\alpha}$ radiation. FTIR

spectra were recorded using a Varian 600 FTIR spectometer. Micro-Raman spectra were recorded on a Jobin Yvon LabRam spectrometer (excitation wavelength: 632.8 nm). Thermogravimetric analysis was carried out using a NETZSCH TG 209 at a heating rate of 20 K min^{-1} under O_2. Electrochemical experiments were performed using two-electrode Swagelok-type cells. For preparing working electrodes, a mixture of the samples of Si@SiO_x/C or pure Si, carbon black, and poly(vinylidene fluoride) (PVDF) at a weight ratio of 70:20:10, was pasted onto pure Cu foil (99.6%, Goodfellow). Glass fibers (GF/D) from Whatman were used as separators. The electrolyte consisted of a solution of 1 M $LiPF_6$ in EC/DMC (1:1 v/v) obtained from Ube Industries Ltd or the same electrolyte containing 2 wt% vinylene carbonate (VC, Aldrich). Pure lithium foil (Aldrich) was used as the counterelectrode. The cells were assembled in an argon-filled glove box. The discharge and charge measurements were carried out on an Arbin MSTAT system. The specific capacity of the Si/SiO_x/C nanocomposites was calculated by using the entire mass of $Si + SiO_x + C$. Electrochemical impedance spectral measurements were carried out over the frequency range from 100 kHz to 10 mHz with ac amplitude of 5 mV on a Solartron 1255 impedance/gain-phase analyzer.

Received: September 17, 2007
Revised: October 17, 2007
Published online: January 21, 2008

Keywords: anode materials · carbon · lithium-ion batteries · nanoparticles · silicon

[1] a) H. S. Zhou, D. L. Li, M. Hibino, I. Honma, *Angew. Chem.* **2005**, *117*, 807 – 812; *Angew. Chem. Int. Ed.* **2005**, *44*, 797 – 802; b) C. Jiang, E. Hosono, H. S. Zhou, *Nano Today* **2006**, *1*, 28 – 33.

[2] A. S. Aricò, P. G. Bruce, B. Scrosati, J. -M. Tarascon, W. van Schalkwijk, *Nat. Mater.* **2005**, *4*, 366 – 377.

[3] a) J. Hassoun, S. Panero, P. Simon, P. L. Taberna, B. Scrosati, *Adv. Mater.* **2007**, *19*, 1632 – 1635; b) G. Armstrong, A. R. Armstrong, P. G. Bruce, P. Reale, B. Scrosati, *Adv. Mater.* **2006**, *18*, 2597 – 2600.

[4] N. S. Ergang, J. C. Lytle, K. T. Lee, S. M. Oh, W. H. Smyrl, A. Stein, *Adv. Mater.* **2006**, *18*, 1750 – 1753.

[5] A. M. Cao, J. S. Hu, H. P. Liang, L. J. Wan, *Angew. Chem.* **2005**, *117*, 4465 – 4469; *Angew. Chem. Int. Ed.* **2005**, *44*, 4391 – 4395.

[6] Y. Wang, J. R. Dahn, *J. Electrochem. Soc.* **2006**, *153*, A2188 – A2191.

[7] a) B. Gao, S. Sinha, L. Fleming, O. Zhou, *Adv. Mater.* **2001**, *13*, 816 – 819; b) M. Green, E. Fielder, B. Scrosati, M. Wachtler, J. S. Moreno, *Electrochem. Solid-State Lett.* **2003**, *6*, A75 – A79; c) J. Graetz, C. C. Ahn, R. Yazami, B. Fultz, *Electrochem. Solid-State Lett.* **2003**, *6*, A194 – A197.

[8] a) H. Li, X. Huang, L. Chen, Z. Wu, Y. Liang, *Electrochem. Solid-State Lett.* **1999**, *2*, 547 – 549; b) G. W. Zhou, H. Li, H. P. Sun, D. P. Yu, Y. Q. Wang, X. J. Huang, L. Q. Chen, Z. Zhang, *Appl. Phys. Lett.* **1999**, *75*, 2447 – 2449; c) X. D. Wu, Z. X. Wang, L. Q. Chen, X. J. Huang, *Electrochem. Commun.* **2003**, *5*, 935 – 939; d) J. Shu, H. Li, R. Yang, Y. Shi, X. Huang, *Electrochem. Commun.* **2006**, *8*, 51 – 54; e) T. Jiang, S. C. Zhang, X. P. Qiu, W. T. Zhu, L. Q. Chen, *Electrochem. Commun.* **2007**, *9*, 930 – 934.

[9] a) J. O. Besenhard, J. Yang, M. Winter, *J. Power Sources* **1997**, *68*, 87 – 90; b) J. Yang, B. F. Wang, K. Wang, Y. Liu, J. Y. Xie, Z. S. Wen, *Electrochem. Solid-State Lett.* **2003**, *6*, A154 – A156; c) W. R. Liu, N. L. Wu, D. T. Shieh, H. C. Wu, M. H. Yang, C. Korepp, J. O. Besenhard, M. Winter, *J. Electrochem. Soc.* **2007**, *154*, A97 – A102.

[10] X. N. Zhang, P. X. Huang, G. R. Li, T. Y. Yan, G. L. Pan, X. P. Gao, *Electrochem. Commun.* **2007**, *9*, 713 – 717.

[11] A. M. Wilson, J. R. Dahn, *J. Electrochem. Soc.* **1995**, *142*, 326 – 332.

[12] T. Umeno, K. Fukuda, H. Wang, N. Dimov, T. Iwao, M. Yoshio, *Chem. Lett.* **2001**, 1186 – 1187.

[13] a) G. X. Wang, J. Yao, H. K. Liu, *Electrochem. Solid-State Lett.* **2004**, *7*, A250 – A253; b) Z. P. Guo, D. Z. Jia, L. Yuan, H. K. Liu, *J. Power Sources* **2006**, *159*, 332 – 335; c) S. H. Ng, J. Wang, D. Wexler, K. Konstantinov, Z. P. Guo, H. K. Liu, *Angew. Chem.* **2006**, *118*, 7050 – 7053; *Angew. Chem. Int. Ed.* **2006**, *45*, 6896 – 6899; d) S. Y. Chew, Z. P. Guo, J. Z. Wang, J. Chen, P. Munroe, S. H. Ng, L. Zhao, H. K. Liu, *Electrochem. Commun.* **2007**, *9*, 941 – 946.

[14] a) I. Kim, P. N. Kumta G. E. Blomgren, *Electrochem. Solid-State Lett.* **1999**, *3*, 493 – 496; b) I. Kim, G. E. Blomgren, P. N. Kumta, *Electrochem. Solid-State Lett.* **2003**, *6*, A157 – A161.

[15] a) M. Holzapfel, H. Buqa, W. Scheifele, P. Novak, F.-M. Petrat, *Chem. Commun.* **2005**, 1566 – 1568; b) M. Holzapfel, H. Buqa, F. Krumeich, P. Novak, F.-M. Petrat, C. Veit, *Electrochem. Solid-State Lett.* **2005**, *8*, A516 – A520.

[16] Y. Liu, K. Hanai, J. Yang, N. Imanishi, A. Hirano, Y. Takeda, *Electrochem. Solid-State Lett.* **2004**, *7*, A369 – A372.

[17] H. Uono, B.-C. Kim, T. Fuse, M. Ue, J.-I. Yamaki, *J. Electrochem. Soc.* **2006**, *153*, A1708 – A1713.

[18] D. Q. Shi, J. P. Tu, Y. F. Yuan, H. M. Wu, Y. Li, X. B. Zhao, *Electrochem. Commun.* **2006**, *8*, 1610 – 1614.

[19] a) T. Zhang, J. Gao, H. P. Zhang, L. C. Yang, Y. P. Wu, H. Q. Wu, *Electrochem. Commun.* **2007**, *9*, 886 – 890; b) J. Saint, M. Morcrette, D. Larcher, L. Laffont, S. Beattie, J. P. Peres, D. Talaga, M. Couzi, J. M. Tarascon, *Adv. Funct. Mater.* **2007**, *17*, 1765 – 1774.

[20] a) L. Chen, K. Wang, X. Xie, J. Xie, *Electrochem. Solid-State Lett.* **2006**, *9*, A512 – A515; b) V. Baranchugov, E. Markevich, E. Pollak, G. Salitra, D. Aurbach, *Electrochem. Commun.* **2007**, *9*, 796 – 800.

[21] a) Q. Wang, H. Li, L. Chen, X. Huang, *Carbon* **2001**, *39*, 2211 – 2214; b) M. M. Titirici, M. Antonietti, A. Thomas, *Chem. Mater.* **2006**, *18*, 3808 – 3812.

[22] a) H. S. Qian, S. H. Yu, L. Luo, J. Gong, X. Liu, L. Fei, *Chem. Mater.* **2006**, *18*, 2102 – 2108; b) M. M. Titirici, A. Thomas, M. Antonietti, *Adv. Funct. Mater.* **2007**, *17*, 1010 – 1018.

[23] C. Meier, S. Luttjohann, V. G. Kravets, H. Nienhaus, A. Lorke, H. Wiggers, *Physica E* **2006**, *32*, 155 – 158.

[24] a) Q. M. Pan, H. B. Wang, Y. H. Jiang, *Electrochem. Commun.* **2007**, *9*, 754 – 760; b) Y. T. Lee, C. S. Yoon, Y. K. Sun, *J. Power Sources* **2005**, *139*, 230 – 234.

[25] D. Aurbach, K. Gamolsky, B. Markovsky, Y. Gofer, M. Schmidt, U. Heider, *Electrochim. Acta* **2002**, *47*, 1423 – 1439.

[26] M. N. Obrovac, L. J. Krause, *J. Electrochem. Soc.* **2007**, *154*, A103 – A108.

